# Virtual experiments provide plausible explanations for IVIVE underpredictions of hepatic clearance

Preethi Krishnan, Andrew K. Smith, Glen E.P. Ropella, Lopamudra Dutta, Ryan C. Kennedy, C. Anthony Hunt

*Bioengineering and Therapeutic Sciences, University of California, San Francisco, CA 94143*

*(P.K., A.K.S., L.D., R.C.K., C.A.H.)*

*Tempus Dictum, Inc., Olympia, WA 98502*

*(G.E.P.R)*

**Abbreviations**: CL, centrilobular; CV, central vein; dPV, distances from portal vein; dCV, distances from central vein; IVIVE, in vitro-to-in vivo extrapolation; MC, Monte Carlo; PV, portal vein; PC, pericentral; PP, periportal; PV, portal vein; SS, Sinusoidal Segment; TS, time step(s); vC1, vCompound-1; vC2, vCompound-2; vC-T, vCompound representing the target drug; vHPC, virtual hepatocyte

## Visual Abstract

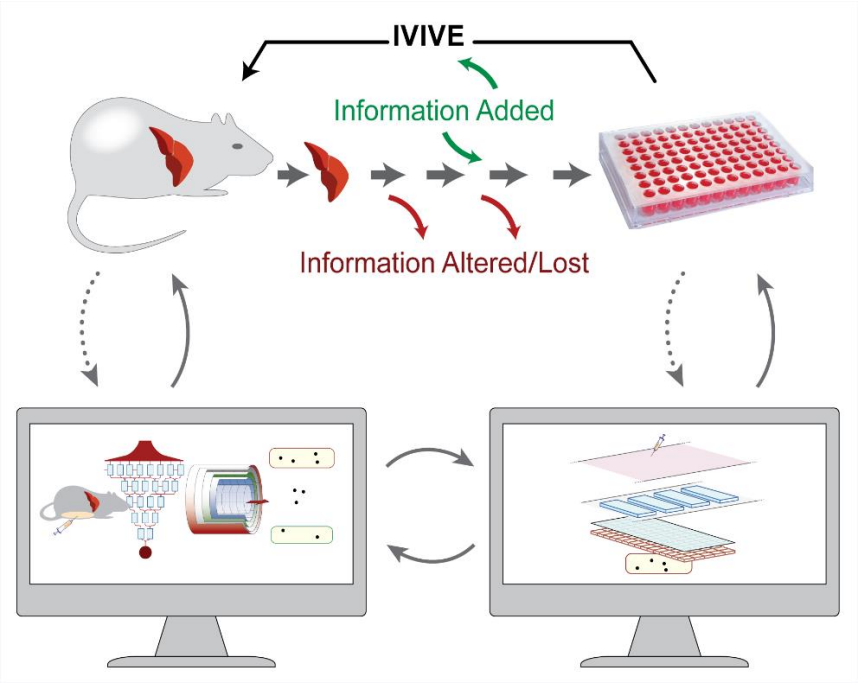

## Abstract

We demonstrate how results of virtual experiments can suggest mechanism-based explanations for IVIVE underpredictions of hepatic clearance. We use agent-oriented, discrete-event methods. We experiment on software analogies of rats and hepatocyte cultures dosed identically with objects that mimic two idealized compounds, vC1 (not cleared) and vC2 (removal maximized). Hepatocytes in cultures and rat livers interact identically with vC1 and vC2. The rules governing vC1 and vC2 movements and interactions with hepatocytes are the same in both systems. The two software systems are independent; to be useful in discovering plausible explanations of IVIVE inaccuracies, we require that, in the absence of hepatocyte exposure differences, the culture-to-rat scaling factor = 1.0 for all corresponding measures. The probability of cell entry (*pEnter*) maps directly to the unbound-fraction of drug used by IVIVE methods. For vC1 (vC2), we achieve that validation target for *pEnter* = 0.05-1.0 (1.0). However, for *pEnter* = 0.05-0.8, vC2 removal rates during culture experiments underpredicted corresponding removal rates in rats. The magnitude of the underpredictions increases with decreasing *pEnter*. For example, using *pEnter* = 0.1 (0.3), peak vC2 removal rates in culture experiments underpredict corresponding removal rates in rats by 3.2 (1.4) fold. Underpredictions are a consequence of the biomimetic periportal-to-pericentral organization of hepatocytes within virtual livers are absent in virtual cultures. In rats, pericentral hepatocytes do more of the vC2 removal work. The results suggest that using IVIVE methods that abstract away influential features of hepatocyte organization within livers may contribute to IVIVE underpredictions.

## Significance Statement

From experiments on virtual (software) counterparts of rats and hepatocyte cultures, we learned that IVIVE underpredictions are a consequence of the biomimetic periportal-to-pericentral organization of hepatocytes within virtual livers being absent in virtual cultures. Using IVIVE methods that abstract away influential features of hepatocyte organization within livers may contribute in part to some IVIVE underpredictions.

## Introduction

Despite continuing research, underprediction of hepatic clearance using in vitro to in vivo extrapolation (IVIVE) methods remains a problem (Bowman and Benet, 2019). Discussions highlight the importance of identifying responsible mechanisms and using that knowledge to develop improved IVIVE methods (Chiba et al., 2009; Wood et al., 2017). However, the realities and uncertainties of working with isolated hepatocytes and scaling derived measures present numerous impediments to disentangling those mechanisms (Wood et al., 2017; Morita et al., 2020). We posit that insights gained from virtual experiments (Kirschner et al., 2014; Petersen et al., 2016; Petersen and Hunt, 2016), using sufficiently biomimetic (realistic) software analogies of hepatic clearance in vivo and clearance by hepatocytes in vitro, may facilitate disentangling those mechanisms.

We have provided evidence supporting the general feasibility of that idea (Smith et al., 2018). We started with virtual mice containing a virtual liver (vLiver) that provided plausible causal mechanism-based explanations for temporal characteristics of acetaminophen hepatotoxicity (Smith et al., 2016). The vLiver contained several thousand quasi-autonomous virtual hepatocytes (vHPCs). Mobile objects represented acetaminophen, its metabolites, and other compounds. Using copies of the vHPCs, we created an independent virtual culture (vCulture) and conducted dose-response experiments using both systems. Temporal measures of toxicity from the two systems were dissimilar, despite acetaminophen metabolism and intra-vHPC toxicity mechanisms being the same. The results provided a resolvable virtual example of an IVIVE disconnect. A root cause of dissimilarities was the hepato-mimetic structural organization of vHPCs within the vLiver that was absent in the vCulture.

A core postulate for IVIVE methods is that, under ideal conditions, the in vitro removal rate (clearance) of unbound drug per hepatocyte (or microsomal equivalents) and the in vivo removal rate of unbound drug per hepatocyte will be equivalent. The virtual counterpart of that postulate serves as a validation target for this work. We envision conducting exploratory virtual experiments using a virtual organism and a vCulture, which utilizes the same vHPCs, to test hypotheses about system differences that may cause virtual compound (vCompound) Removal rates in one system to differ significantly from those in the other system. An essential requisite for achieving that vision is that we provide evidence of achieving the validation target using both virtual systems.

We use a vCulture and virtual organism that include new features and meet new requirements. The virtual organism maps to a typical rat. The vCulture maps to cultured hepatocytes from the same rat type. We study two simple, highly permeable vCompounds that represent the hypothetical extremes for in vitro and in vivo hepatocyte removal of xenobiotics. vCompound-1 (vC1) enters and exits all vHPCs but is neither removed nor metabolized. vCompound-2 (vC2) experiences maximal removal; it enters but does not exit vHPCs. The parameters and rules governing extracellular vCompound movements are the same in both systems. vCompound amounts and dosing are the same in all experiments. To explain differences in vCompound dynamics between the two systems, we define and measure vHPC exposure rates. For vC1, vHPC exposure rate = vHPC entry events per time step. For vC2, vHPC exposure rate = removal rate. The parameter *pEnter* maps to the unbound fraction of the drug. It specifies the probability that a vCompound adjacent to a vHPC will enter when given the opportunity to do so.

In experiments using vC1, for *pEnter* = 0.05-1.0, exposure rates in vCulture and in vRats are equivalent, providing evidence that the validation target is achieved.

In experiments using vC2, with *pEnter* = 1.0, peak removal rates in vCulture and in vRats are equivalent, providing evidence that, for *pEnter* = 1.0, the validation target is achieved. However, for *pEnter* = 0.05-0.8, peak removal rates in vCulture underpredicted corresponding removal rates in vRats. The magnitude of the underprediction increases with decreasing *pEnter*. For example, using *pEnter* = 0.1 (0.3), the vRat-to-vCulture ratio of peak vC2 removal rates = 3.2 (1.4). Those differences are a consequence of the biomimetic organization of vHPCs within vLivers being absent in vCultures. Within vLivers, removal rates increase periportal-to-pericentral, whereas the influence of *pEnter* decreases periportal-to-pericentral. Those results suggest that use of IVIVE methods that abstract away influential features of hepatocyte organization within lobules may contribute in part to some IVIVE underpredictions.

Achieving the validation target for vC1 and vC2 corroborates that vCompound disposition dynamics within vCultures and vRats can be made strongly analogous to in vitro and in vivo counterparts. The results support the idea that exploratory experiments using vCultures and vRats can identify mechanism-based differences in vHPC removal rates that may account for IVIVE underpredictions of hepatic clearance.

## Methods

We use discrete-event simulation methods. To distinguish key virtual system components from real counterparts, we append the prefix "v" and to distinguish virtual characteristics and phenomena from real counterparts, we capitalize the former. The components of virtual experiments and methods are similar to those described in recent reports (Smith et al., 2016; 2018; 2020; Peterson et al., 2016).

The hepatic clearance of a drug is often defined as the volume of blood that is cleared of the drug by the liver per unit of time. As described below, a vLobule (Fig. 1) contains spaces, which may contain vCompounds. Blood flow is simulated. There is no software counterpart to the volume of blood. In this work, the virtual counterpart to hepatic clearance is (vLiver) Removal rate, which is the amount of vCompound removed by the vLiver during each time step.

This work is conditioned on four postulates: 1) The structural organization of vHPCs within the vLobules (Fig. 1) is strongly analogous to the histological organization of hepatocytes within rat and human lobules (Teutsch et al., 1999; Teutsch, 2005; Smith et al., 2020). 2) vHPC components and vCompound removal mechanisms are concrete, biomimetic, and strongly analogous to counterparts in vivo and in vitro (Smith et al., 2018, 2020; Peterson et al., 2016; Hunt et al., 2011). 3) The structural organization of vHPCs within vCultures is sufficiently biomimetic to simulate the in vitro experiments used to derive measures of intrinsic clearance (Petersen et al., 2016; Smith et al., 2018). 4) When averaged over many events and many Monte Carlo-sampled executions (hereafter, simply executions), measures of vCompound dynamics within and between spaces in vLobules (and vCultures) can scale quantitatively to match comparable measurements of actual chemical entities, within wet-lab measurement errors (Smith et al., 2020).

A core postulate for IVIVE methods is that, under ideal, comparable conditions, the in vitro removal rate (clearance) of unbound drug per hepatocyte (or microsomal equivalents) and the in vivo removal rate of unbound drug per hepatocyte will be equivalent. The virtual counterparts of that equality are our quantitative cross-system validation targets (Sargent, 1999) (see *vCompound Exposure and Removal Rates*).

Because rats are often the referent system for IVIVEs, the virtual organism is vRats. The vLobules in Fig. 1 have no properties (parameters, components, variables, or logic) that will differ if they are mapped to mouse, rat, or human hepatic lobules. Similarly, there are no properties of vHPCs (components, parameters, variables, or logic) that will differ if they are mapped to mouse, rat, or human hepatocytes.

### *Virtual experiments, model mechanisms, and requirements*

Because all wet-lab experiments are concrete, our virtual experiment approach involves building, experimenting on, and iteratively refining biomimetic model mechanisms constructed using software components (Kirschner et al., 2014; Petersen and Hunt, 2016). Model mechanisms differ fundamentally from equation-based pharmacokinetic and clearance models employed by conventional IVIVE methods (Hunt et al., 2018). During execution, model mechanisms generate phenomena which, when measured, may be qualitatively and quantitatively similar to corresponding measures of wet-lab phenomena. The vRat and vCulture systems meet the following requirements

1. A virtual mechanism exhibits the same characteristics as an explanatory biological mechanism (Darden, 2008). Specifically, it has a context, and its components (modules, entities, and activities) are arranged spatially and exhibit structure, localization, orientation, connectivity, and compartmentalization. vCompound dynamics, mediated by model mechanisms, have temporal aspects, including rate, order, and duration.
2. Components and spaces are concrete, parsimoniously biomimetic (Hunt et al., 2011), and sufficiently modular to facilitate analogical reasoning (Bartha, 2013, Frigg and Hartmann, 2012).
3. A vCompound type can map to a particular chemical entity. Quasi-autonomous components (i.e., software agents such as a Sinusoidal Segment and vHPCs) recognize different vCompound types and adjust their responses appropriately. For example, a vHPC recognizes that an adjacent vCompound has the property *membraneCrossing* = yes and allows it to enter stochastically.

### *Virtual Rats, Livers, Lobules, Sinusoidal Segments, and Cells*

Model execution is a discrete-event Monte Carlo (MC) simulation. One vRat Experiment is a fixed number of executions—12 in this work—of the system illustrated in Fig. 1, with a different pseudo-random number seed for each execution. A vRat (Fig. 1) comprises a vLiver (detailed below), Rat Body, and a space to contain Dose for simulating intraperitoneal (or oral) dosing. In this work, a vLiver = 12 Monte Carlo (MC)-sampled vLobules. One MC-sampled vLobule maps to a small random sample of possible lobular flow paths within a whole liver along with all associated tissue volume. A vLobule is a coarse analogy of an actual rat and human lobule (primary hepatic unit) (Teutsch et al., 1999; Teutsch

2005). A directed acyclic graph with a Sinusoidal Segment (SS) object at each graph node. Flow follows the directed graph edges connecting SSs. Flow paths map to a conflation portal and septal sinusoids.

A quasi-3D SS object is a software agent. It comprises a Core and five 2D grids arranged concentrically: Blood-Cell Interface, Endothelial Cell Space, Space of Disse, Hepatocyte Space, and a Bile space (not used in this work). During execution a SS functions as an analog of sinusoid components and features averaged across many actual lobules; SS dimensions are MC-sampled within constraints at the start of each Experiment to mimic lobular variability and simulate a wide variety of periportal (PP) to pericentral (PC) flow paths. The Portal Vein (PV) is connected to all Layer 0 SS. From PV to Central Vein (CV), there are 45, 25, 20, 15, and 9 SS per Layer. There are 55 Layer 0-to-1 edges; 65 Layer 1-to-2; 35 Layer 2-to-3, and 25 Layer 3-to-4 edges. A graph edge connects each Layer 5 SS to CV. There are also intra-Layer edges (randomly assigned for each execution), which mimic connections between sinusoids: 20 within Layer 0, 7 within Layer 1, 5 within Layer 2, 2 within Layer 3, and 0 within Layer 4. Having more edges than SSs mimics the wide variety of PV-to-CV flow paths within hepatic lobules. Interconnections are essential to enable the same vLiver to achieve previously described pharmacokinetic validations for several different drugs (Yan et al., 2008, Smith et al., 2016). Numbers of intra- and inter-Layer edges are fixed for all Experiments, but their particular SS-to-SS connections are Monte Carlo-sampled for each execution.

For this work, we increased Layers (from three to five), number of SSs (from 68 to 144), number of graph edges, and reduced mean SS circumferences and lengths by approximately 50%, while maintaining carrying capacity. Those changes improved hepatic disposition biomimicry, specifically they improved vCompound lateral dispersion and reduced the parallel nature of SS flow paths in Layer 2 (third Layer) of the 3-Layer graph structure. The structure detailed above was achieved by following the Iterative Refinement Protocol (Lam and Hunt, 2010; Smith et al., 2016; Kennedy et al., 2018) to achieve qualitative and quantitative cross-validation between measures of Marker dynamics (described below) and measures of acetaminophen hepatotoxicity.

Cell objects are software agents. They mediate all interaction with vCompounds, including entry and exit, based on the properties of each vCompound type. Cells occupy 99% Endothelial Cell Space and all of Hepatocyte Space. Other Cell object types can be included when required, but they were not needed for this work. Both Endothelial Cells and vHPCs contain binder objects to simulate non-specific binding.

They map to a conflation of all epithelial cell components responsible for non-specific binding of a referent compound. A vHPC object does not map 1:1 to a hepatocyte. Rather, a vHPC at a particular PV-to-CV location in Hepatocyte Space maps to a conflation of relevant hepatocyte functionality at a corresponding relative PV-to-CV location. However, events occurring within a particular vHPC do map directly to corresponding events believed to occur within hepatocytes at a comparable location. vHPCs contain four types of physiomimetic modules to control material entry, removal, binding and transformations needed to simulate acetaminophen hepatotoxicity (Smith et al., 2020): *EliminationHandler*, *MetabolismHandler*, *BindingHandler*, and *InductionHandler*. Although not used for this work, these modules represent a conflation of all relevant hepatocyte functionality that referent compound encounters after entering hepatocytes. The mean number of vHPCs per execution = 8,475 (SD = 167). The mean numbers of vHPCs at different PV-to-CV locations are illustrated in Fig. 2A.

### *Simulation time and vCompounds*

During execution, time advances in discrete time steps (TS; also called simulation cycles). The duration of each execution is 21,600 TS. During previous virtual acetaminophen hepatotoxicity experiments, one TS mapped to one second (Smith et al., 2020). The mapping of TS to clock wet-lab time for a pharmacokinetic study in rats may be different (e.g., 1 TS = 4 seconds). For this work, no particular mapping is required. In discrete-event simulations, all scheduled events occur at a particular instant in time, marking a change of system state. Measures of component states at the end of each simulation cycle, averaged over all executions, may map (qualitatively or quantitatively) to corresponding wet-lab measures. However, the events occurring during a TS have no direct wet-lab counterparts. Rather, they are intended to be analogous to the net consequences of fine grain processes occurring in parallel within wet-lab counterparts. To simulate the parallel nature of actual fine grain processes, the order of events is randomized for each TS.

We use three vCompounds, Marker, vC1, and vC2. The Dose for each Experiment is 100,000 vCompounds. A vCompound object maps to a tiny fraction of a referent drug dose. In vRat Experiments, a fraction of Dose (in the initial Dose space) is transferred to Rat Body, simulating first order absorption following intraperitoneal (or oral) dosing. For convenience, we reused the simulated absorption rate used for acetaminophen (Smith et al., 2016). Marker is always 50% of each Dose. It serves as a multi-attribute virtual internal standard of vCompound disposition by interacting inertly with the vLobule (or

vCulture) structure. It behaves somewhat analogous to sucrose. It does not enter Cells (parameter *membraneCrossing* = false). For vC1 and vC2, *membraneCrossing* = true. Absent structural changes, Marker behavior during repeat executions of the same system type is invariant. Marker is particularly useful during cross-validation Experiments and during verification Experiments following code changes. Its use is explained further in (Smith et al., 2020).

### *vCompound Exposure and Removal rates*

We measure the number of vHPC Entry and Exit events during each TS. To be exposed to the vHPC's Metabolizing components, a vCompound must enter the vHPC. Thus, an Entry event is defined as one vHPC Exposure event, and vHPC Exposure rate (simply Exposure rate hereafter) = Entry events per vHPC per TS.

The consequence of a Cell's interaction with vC1 or vC2 is determined by the parameter *cellEnterExitProb*. Each TS, when *membraneCrossing* = true, a vCompound adjacent to Cell is given a stochastic opportunity to enter (or not). The subsequent occurrence of an Entry event is determined by the probability of Entry, *pEnter*. Each TS, an unbound intra-Cellular vCompound is given the stochastic opportunity to exit (or not). The subsequent occurrence of an Exit event is determined by the probability of exiting, *pExit*. For vC1, *pExit* = 1.0 (high permeability). vC1 is not removed. For vC2, *pExit* = 0. Consequently, for vC2, Exposure rate = Removal rate. Its Removal rate is the maximum for the vRat and vCulture configurations employed. To characterize location-dependent differences in events, we average the measures over the MC trials within the Periportal (PP), Centrilobular (CL), and Pericentral (PC) bands illustrated in Fig. 2A.

The virtual counterpart of the core postulate for IVIVE methods is the following requirement. Absent significant vRat-vCulture differences in intra-vHPC mechanisms and vHPC accessibility, and under comparable dosing conditions, the mean Exposure rate of a highly permeable unbound vCompound will be equivalent in both systems. Thus, differences in vCompound disposition between the two systems can be attributed to differences in vHPC organizatiol and accessibility with the vLobule and vCulture that are independent of vCompound properties.

Two specific cases of the core postulate serve as validation targets. 1) Under dynamic steady-state conditions and within the variance of the executions, the systemwide mean vHPC Exposure rates for vC1

are equivalent in vRats and vCulture. 2) When using *pEnter* = 1 and comparable dosing conditions, and within the variance of the executions, the systemwide mean vHPC Exposure rates for vC2 are equivalent in vRats and vCulture.

To alter vHPC accessibility, we change the value of *pEnter* and use measures of Exposure and Removal rates to assess the consequences. Decreasing values of *pEnter* map directly to decreasing the unbound fraction of drug used in IVIVE methods. Decreasing values of *pEnter* can also map to a decrease in effective partition coefficient or a decrease in effective hepatocyte permeability.

### *vCompound dynamics within vLobules*

During a vRat Experiment, vCompounds enter the vLobule from Rat Body via the PV. To mimic the consequences of hepatic blood flow, a fraction of all vCompounds in Rat Body is moved to PV each TS. For all results reported below, that fraction is the same as used by Smith et al. (2020) to simulate hepatic blood flow. Each TS, vCompounds in PV are moved randomly to the Core or Interface spaces in Layer-0 SSs. vCompounds exiting a SS via Core and Interface Space are moved to a lateral or downstream SS along a randomly selected connecting graph edge. Within a SS, vCompounds percolate stochastically through accessible extra-Cellular spaces influenced by three local flow parameters. Simulated blood flow in the Core is controlled by *ssFlowRate*. Outside the core, extracellular movement is a biased random walk controlled by the values of *forwardBias* and *lateralBias* listed in Supplemental Table. Those parameter values are the same for vC1, vC2, and Marker. vCompounds that exit a Layer-4 SS to the CV are returned to Rat Body. Measurements of vCompound in Rat Body can map quantitatively to measures of a referent drug in plasma (or blood). vLiver Extraction Ratio (measured each TS) = (amount of vCompound in PV – amount in CV) / amount in PV.

### *Virtual Culture*

At the start of a execution, all components are created, assembled, parameterized, the Experiment protocol is initiated, and measurements begin. To minimize coded differences in that process between a vRat and a vCulture Experiment, the vCulture illustrated in Fig. 2B is a partially deconstructed variant of a vRat (and its vLobule). The well-mixed Rat Body space is retained and renamed Media Space. The vLobule's directed graph structure is reduced to one Layer of SSs connecting PV to CV. That node is occupied by the same number of SSs in the vLobule (114 SSs), but vCulture uses the reduced version of

the SS in Fig. 2B. All vCulture SS objects are confined to a space that corresponds to Layer 0 in Fig. 1. For simplicity, all SSs are the same size: 15 (w) x 5 (l) grid spaces with vHPCs assigned to each grid point, for total of 8,550 vHPCs for each execution (vs. a mean of 8,475 in vRat Experiments).

The SS Core, Endothelial Cell Space (plus Endothelial Cells), the Space of Disse, and the Bile Space are removed but the Hepatocyte Space (plus vHPCs) is retained. The Blood-Cell Interface Space, PV, and CV in Fig. 1 are combined to function as the Media-Cell Interface Space. Each TS, a fraction vCompound in Media Space is transferred randomly to Media-Cell Interface grids. From there vCompounds move to and within Hepatocyte Space. They may enter and exit vHPCs exactly as they do within vLobules. Manipulating the properties of the Media-Cell Interface Space can map to the unstirred water layer (Wood et al., 2018). Manipulating its properties may provide a means to explore and test hypotheses about plausible influences of the unstirred water layer on measures of in vitro clearance.

In vRat Experiments, we simulate first order absorption following intraperitoneal (or oral) dosing. To simplify graphical comparisons of vRat and vCulture measures, Dose is metered into Media Space so that peak Times for percent Dose in Media Space and in Rat Body for vC2, with *pEnter* = 1, were the same, within measurement variance.

### *Making virtual measurements analogous to wet-lab measurements*

We measure virtual features and phenomena analogous to how corresponding wet-lab measurements are (or might be) made. Doing so strengthens the virtual-to-wet-lab experiment analogy. Many parameters are probabilistic. Several feature specifications are Monte Carlo-sampled at the start of each execution. Measurements are averaged over 12 executions per Experiment. Consequently, measurements often exhibit considerable variability. That variability is intentional. It represents and helps account for the variability and uncertainty that characterizes targeted wet-lab measurements.

### *Component biomimicry has limits*

None of the objects in Fig. 1 are intended to model actual biological counterparts explicitly. Rather, their organization, function, and behaviors during execution—the model mechanisms—are intended to be sufficiently analogous to their biological counterparts so that prespecified fine- and coarse-grain measures, recorded during executions can map quantitatively to prespecified validation targets (Hunt et

al., 2018). When that evidence is available, then the model mechanism stands as a plausible, tested model of explanation for how the target phenomena was generated.

A SS does not map directly to a portion of a single sinusoid and adjacent tissue. Rather, events occurring within a particular SS are intended to be parsimonious yet strongly analogous to referent events. The mapping from cylindrical 2D Hepatocyte Space to corresponding 3D configurations of hepatocytes is an approximation. Because a SS does not map directly to a portion of a single sinusoid, a vHPC at a particular Hepatocyte Space grid point maps to a conflation of relevant hepatocyte functionality accessed by referent drug at a corresponding relative PV-to-CV location during a rat experiment or at an arbitrary location in vitro. Thus, a vHPC cannot map 1:1 to a hepatocyte, although there are strong functional analogies. It follows that a vLobule does not model liver anatomy or lobular microanatomy, yet its contribution to the model mechanism can be hepato-mimetic during execution.

### *Hardware and software details*

The Java-based MASON multi-agent toolkit was used to develop the vLiver and vCulture. Experiments were executed using local hardware running 64-bit Linux Mint and Google compute engine was used as the virtual machine. The virtual framework was created using Java. The R programming language was used for analyses and plotting data. vRats, vCultures, and configuration files are managed using the Subversion version control tool in two repositories, one private (Assembla) and another public. Values for key vHPC specifications and parameterizations are listed in Supplemental Table. Quality assurance and control details, along with practices followed for validation, verification, sensitivity analyses, and uncertainty quantification are as discussed in (Smith et al., 2016). The toolchain, operating system, configurations, and our entire code base is available on (https://simtk.org/projects/isl/).

## Results

Dose rate and vHPC numbers are closely matched for vCulture and vRat Experiments. Within corresponding grid spaces, vC1 and vC2 movements during each TS are governed by the same rules. Consequently, when using the same *pEnter*, the vCulture-to-vRat scaling factor = 1.0. Thus, corresponding vCulture and vRat measures are directly comparable.

### *Experiments using vC1*

Mean measures of vC1 disposition dynamics during vCulture and vRat Experiments are provided in Fig. 3 and Fig. 4. To match Experiment conditions, and to simplify comparisons between the two systems, the delivery rate of vC1 to the vCulture Media Space is adjusted, as described in Methods, to correspond to the simulated first order absorption used for the vRat Experiments. Consequently, the mean percent Dose in Media and Rat Body under dynamic steady-state conditions is comparable. In both systems, mean dynamic steady-state vHPC Exposure rates increase with increasing values of *pEnter* (0.05-1.0). For smaller *pEnter* values, the increase is convex, transitioning to linear. In both systems, within the variance of the executions, mean vHPC Exposure rates and mean dynamic steady-state values for percent Dose in vHPCs are equivalent. Thus, the validation target is achieved for vC1.

### *Experiments using vCompound-2*

Measures of vC2 disposition dynamics during vCulture and vRat Experiments are provided in Fig. 5 and Fig. 6. For vC2, Exposure rate = Removal rate. Hereafter, we use Removal rate when referring to vC2. The temporal profiles for percent dose in Media and Rat body and vHPC Removal rates are equivalent for *pEnter* = 1.0, within the variance of the executions. Thus, a vC2 validation target is achieved. However, those measures are not equivalent for *pEnter* = 0.05-0.8. As *pEnter* decreases, the magnitude of differences between identical measures recorded during vCulture and vRat Experiments increases.

In vCultures, the decrease in percent Dose in Media with increasing *pEnter* is somewhat nonlinear (Fig. 5A). That nonlinearity is reflected in Removal rates (Fig. 5B), Extraction ratios (Fig. 5C), and cumulative Removal (percent Dose in vHPCs, Fig. 5D).

In vRat (Fig. 6A-D), the nonlinearities are more pronounced. Percent Dose in Rat Body, Removal rates, and cumulative Removal are relatively robust to changes in *pEnter* within the 0.5-1.0 range. The mean Extraction for *pEnter* = 1.0 and 0.8 are equivalent, within the variance of the executions.

At corresponding times, for *pEnter* = 0.05-0.5, peak Removal rates in vCulture (Fig. 5B) considerably underpredict corresponding peak Removal rates in vRats (Fig. 6B). Likewise, at corresponding times, cumulative Removal in vCulture (Fig. 5D) considerably underpredicts corresponding cumulative Removal in vRat (Fig. 6D).

The divergence of measures of peak Removal rates between vCulture and vRat Experiments as *pEnter* decreases from 0.8 to 0.05 is a consequence of the biomimetic structural organization of vHPCs within vLivers being absent in vCultures. During vCulture Experiments, the mean vC2 Removal rates, averaged over many executions, are the same for all vHPCs. However, the results in Fig. 6E-G show that those measures are not the same for vLiver vHPCs. They depend on vHPC location within vLivers. That location dependency is a consequence of the combined impact of two features, upstream Removal of vC2 and the PP-to-PC decrease in the number of vHPCs (Fig. 2A). The magnitude of the PP-to-PC differences increase with decreasing *pEnter*. To illustrate, for *pEnter* = 1.0, the PC/PP ratio for peak Removal rates is 1.4, yet for *pEnter* = 0.05, the ratio is 3.5. For cumulative Removal at $t$ = 7,500 TS, the PC/PP ratio for *pEnter* = 1.0 is 1.5, whereas, for pEnter = 0.05, it is 2.8.

The *pEnter*-dependent patterns within the three bands in Fig. 6E-G are a consequence of the temporal mixing of Mechanism features changing PP-to-PC. In both vCulture and vRat Experiments, a step-like pattern is evident in post-peak measures of Removal rate (Fig. 5B and Fig. 6B). That is a consequence of specifying that the mean SS length in vRat Experiments be approximately 5 grid points, the same as all reduced SSs used by vCulture. That was done to facilitate comparing results of vCulture and vRat Experiments. When SS length is sampled from a wider distribution, that step-like pattern vanishes (Smith et al., 2016).

## Discussion

This work focuses on the four-stage working thesis illustrated in Fig. 7. We first provide a summary of the thesis and then expand on the three stages utilizing simulation. In stage A, an IVIVE method is used to predict the hepatic clearance of a target drug, but the actual value is underpredicted, e.g., by a factor of ≥ 2x. The likely explanation is that the IVIVE method was based on an overly simplified theory. Thus, to reduce such prediction bias, one or more new mechanism-based theories are needed. Using a vCompound to represent the target drug (vC-T), the goal for stage B is to develop and verify a plausible analogically mechanism-based explanation of the in vitro clearance data. Using the same vC-T, the goal for stage C is to develop and verify a plausible analogical mechanism-based explanation of the in vivo hepatic clearance data. Insights gained from B and C are then used in stage D to provide a plausible explanation for the underprediction, which may suggest an improved IVIVE method for subsequent use.

Parts B and C are independent. The objective of stage B is to discover parsimonious vCulture, vHPCs, and vC-T parameterizations that establish quantitative mappings between in vitro measures of the target drug's removal and corresponding measures of vC-T removal during vCulture executions that meet prespecified validation targets. Doing so requires cycling many times through the Iterative Refinement Protocol cited in Methods (Lam and Hunt, 2010; Petersen et al., 2016; Kennedy et al., 2019). The initial stages involve falsification of early model mechanism hypotheses. Petersen et al. (2016) detail examples of the stage B process.

The objective of Part C is to establish quantitative mappings between measures of vC-T disposition during vRat (or another virtual animal) executions and corresponding in vivo measures of the target drug's hepatic clearance. That process also requires Iterative Refinement Protocol cycling to discover parameterizations of the vRat, vLobule, vHPCs, and vC-T that enable measures of vC-T's disposition to map quantitatively to in vivo counterparts. Yan et al. (2008) and Smith et al. (2016) detail examples of the stage C process.

We have complete, independent control over the vCulture and vRat systems and their Mechanisms. The uncertainties associated with the wet-lab experiments are absent. However, because stages B and C are independent and because the vRat and vCulture systems are created separately, there is ample opportunity for introducing bias, such as programming inadvertent differences into mechanism details that influence vC-T dynamics differently within the two systems in ways that have no wet-lab counterparts. Any

evidence of such flaws weakens the four-stage working thesis, and the supported analogical. Completing preplanned verification tests helps avoid such flaws. Results confirming that the two essential vC1 and vC2 validation targets have been achieved provides strong evidence that, within the variance of the executions, no significant inadvertent differences have been discovered. vC1 and vC2 can serve as reference controls for stage D. Their behaviors provide minimal background mechanisms against which to compare the more complicated disposition dynamics of vC-T, somewhat analogous to Marker uses described in Methods.

Because differences in vC-T's behaviors in stages B and C are entirely explainable, results from stage D may provide scientifically useful new knowledge. We can observe, measure, and explain the unfolding of disposition details during vRat and vCulture executions. From that information, we can develop one or more verifiable explanations for differences in vC-T's dynamics within the two systems. Those explanations can stand as plausible concrete semi-quantitative theories for how and why the IVIVE method failed. Key features of such a theory may then be targeted for challenge using narrowly focused wet-lab experiments. No matter the outcome of those experiments, we will have useful new knowledge for improving the IVIVE method.

Dose rate and vHPC numbers are closely matched for vCulture and vRat Experiments. Within corresponding grid spaces, vCompound movements during each TS are governed by the same rules. Consequently, when using the same *pEnter*, the vCulture-to-vRat scaling factor = 1.0 for all corresponding measures. For those cases where validation is achieved, vCulture measures directly predict corresponding vRat measures. The results provide other cases where vCulture measures fail to predict corresponding vRat measures. They consistently underpredict. Below, we present and explain examples.

Under dynamic steady-state conditions, mean extra-Cellular amounts of vC1 are uniform in both systems. For each *pEnter*, the systemwide mean vHPC Exposure rates (Fig. 3B and Fig. 4B) are equivalent, within the variance of the executions. However, during vRat Experiments, mean Exposure rates (Fig. 4D) and thus mean amounts of vC1 per vHPC (Fig. 4F) increase PP-to-PC. The differences are most dramatic for *pEnter* = 1.0. That characteristic is noteworthy because IVIVE methods typically employ either the well-stirred or parallel tube liver models. Both models predict that all vHPCs experience the same vC1 Exposure rates under dynamic steady-state conditions.

For vC2 using *pEnter* = 1.0, measures of Removal from Media (Fig. 5A) and mean peak Removal rates (Fig. 5B) accurately predict corresponding measures in vRat Experiments (Fig. 6A and 6B), within the variance of the executions. However, for *pEnter* ≤ 0.8, those vCulture measures underpredict corresponding vRat values. The magnitude of the underprediction increases dramatically with decreasing *pEnter*. For *pEnter* = 0.3 (0.1), the peak Removal rate is underpredicted by a factor of 1.4x (3.2x). Those underpredictions, which we elaborate below, trace directly to the structured organization of vHPCs within vLobules, which is absent in vCultures.

Because we measure amounts of vC2 entering and exiting Media-Cell Interface space each TS, we can calculate vCulture Extraction ratios (Fig. 5C). Extraction ratio vs. *pEnter* is slightly nonlinear (Fig. 5C, right side). That nonlinearity is more evident in the plot of mean peak Removal rate vs. *pEnter* (Fig. 5B, right side). Those nonlinearities are also evident in the percent Dose in Media profiles (Fig. 5A) and the cumulative removal profiles (Fig. 5D). In all four cases, nonlinearities are a consequence of the variety of randomized events involving vC2 that occur between entering and exiting Media-Cell Interface space. vC2 participates in only one event per TS, and only one of those events—entering a vHPC—is influenced by *pEnter*. The net consequence of those events is strongly analogous to the unstirred water layer effect described by Wood et al. (2018).

The nonlinearities in vRat Experiments are more dramatic than those in vCulture. Because PV-to-CV path lengths are much longer, the influence of *pEnter* is diminished further. Hence, the temporal profiles of percent Dose in Rat Body (Fig. 6A) and cumulative Removal (Fig. 6D) are relatively robust to changes in *pEnter* within the range 0.2-1.0, unlike the corresponding vCulture profiles. Likewise, the peak Removal rates (Fig. 6B) and Extraction Ratio measures (Fig. 6C) are relatively robust to changes in *pEnter* within the range 0.5-1.0. The intra-Lobular measures in Fig. 6E-G bring into focus how the structural organization of vHPCs within vLobules contributes to that robustness. The consequences of changing *pEnter* on peak Removal rates and cumulative Removal are strongest within the PP band. The influence of *pEnter* diminishes as vC2s traverses the CL band, and it is almost absent for vC2s traversing the PC band. Although the amounts of vC2 removed within the three bands decrease PP-to-PC (Fig. 6F), the per vHPC Removal rates, and thus per vHPC amounts, increase PP-to-PC, which means that the PC vHPCs do more of the vC2 removal work, unlike in vCultures.

The expression levels of the majority of liver genes responsible for detoxification and xenobiotic metabolism increase PP-to-PC (Halpern et al., 2017). We infer that, for xenobiotics primarily cleared by those enzymes, the underprediction resulting from abstracting away hepatocyte organization within the liver will be amplified. Such mechanism-based synergy may help explain why medium-to-high clearance predictions for compounds that are metabolized by cytochrome P-450 enzymes are often underestimated using conventional IVIVE methods. Further work is needed to challenge that conjecture.

In this work, we sought a balance between more detailed biomimicry and the computation programmed into vRat and vCulture model Mechanisms. Previous reports detail strengths, limitations, and weaknesses of the analogical approach and methods used herein (Hunt et al., 2009; 2011; 2018; Petersen et al., 2016; Smith et al. 2016). We argue that, because of measurement limitations and the fog of multi-source uncertainties impacting IVIVEs, increased reliance on analogical reasoning and arguments is necessary to make progress disentangling mechanisms contributing to IVIVE inaccuracies. Reliance on analogical arguments and reasoning is both a limitation and strength (Frigg and Hartmann, 2012). Bartha provides guidelines for assessing the scientific strengths and limitations of analogical arguments (Bartha, 2019).

The results support the idea that exploratory Experiments using vCultures and vRats can identify mechanism-based differences in vHPC removal rates that may account for IVIVE underpredictions of hepatic clearance. We suggest that IVIVE methods can be improved by utilizing a liver model, such as the vLiver employed here, that couples a biomimetic representation of the structural organization of HPCs with biomimetic representations of Intrahepatic vCompound dynamics.

## Acknowledgements

We thank the authors of the MASON simulation toolkit and also the creators of the SimTK project-hosting platform for facilitating development and distribution of this project.

## Author contributions

*Participated in research design*: PK, AKS, GEPR, CAH

*Conducted experiments*: PK, AKS, GEPR, LD

*Contributed analytic tools*: PK, AKS, GEPR

*Performed data analyses*: PK, AKS, GEPR, CAH

*Wrote or contributed to the writing of the manuscript*: PK, AKS, GEPR, LD, RCK, CAH

## References


Bartha P (2013) Analogy and Analogical Reasoning. *The Stanford Encyclopedia of Philosophy*. https://plato.stanford.edu/archives/fall2013/entries/reasoning-analogy/.

Bowman CM, and Benet LZ (2019) In Vitro-In Vivo Extrapolation and Hepatic Clearance-Dependent Underprediction. *J Pharm Sci* 108:2500–2504.

Chiba M, Ishii Y, and Sugiyama Y (2009) Prediction of hepatic clearance in human from in vitro data for successful drug development. *AAPS J* 11:262–276.

Darden L (2008) Thinking Again about Biological Mechanisms. *Philosophy of Science* 75:958–969.

Frigg R, and Hartmann S (2012) Models in Science. *The Stanford Encyclopedia of Philosophy*. https://plato.stanford.edu/archives/fall2012/entries/models-science/.

Halpern KB, Shenhav R, Matcovitch-Natan O, Toth B, Lemze D, Golan M, Massasa EE, Baydatch S, Landen S, Moor AE, Brandis A, Giladi A, Avihail AS, David E, Amit I, and Itzkovitz S (2017) Single-cell spatial reconstruction reveals global division of labour in the mammalian liver. *Nature* 542:352–356.

Hunt CA, Ropella GEP, Lam TN, Tang J, Kim SHJ, Engelberg JA, and Sheikh-Bahaei S (2009) At the biological modeling and simulation frontier. *Pharm Res* 26:2369–2400.

Hunt CA, Ropella GEP, Lam T ning, and Gewitz AD (2011) Relational grounding facilitates development of scientifically useful multiscale models. *Theor Biol Med Model* 8:35.

Hunt CA, Erdemir A, Lytton WW, Mac Gabhann F, Sander EA, Transtrum MK, and Mulugeta L (2018) The Spectrum of Mechanism-Oriented Models and Methods for Explanations of Biological Phenomena. *Processes* 6(5):56.

Kennedy RC, Smith AK, Ropella GEP, McGill MR, Jaeschke H, and Hunt CA (2019) Propagation of Pericentral Necrosis During Acetaminophen-Induced Liver Injury: Evidence for Early Interhepatocyte Communication and Information Exchange. *Toxicol Sci* 169:151–166.

Kirschner DE, Hunt CA, Marino S, Fallahi-Sichani M, and Linderman JJ (2014) Tuneable resolution as a systems biology approach for multi-scale, multi-compartment computational models. *Wiley Interdiscip Rev Syst Biol Med* 6:289–309.

Lam TN, and Hunt CA (2010) Mechanistic insight from in silico pharmacokinetic experiments: roles of P-glycoprotein, Cyp3A4 enzymes, and microenvironments. *J Pharmacol Exp Ther* 332:398–412.

Morita K, Kato M, Kudo T, and Ito K (2020) In vitro-in vivo extrapolation of metabolic clearance using human liver microsomes: factors showing variability and their normalization. *Xenobiotica* 50:1064–1075.

Petersen BK, Ropella GEP, and Hunt CA (2016) Virtual Experiments Enable Exploring and Challenging Explanatory Mechanisms of Immune-Mediated P450 Down-Regulation. *PLoS ONE* 11:e0155855.

Petersen BK, and Hunt CA (2016) Developing a vision for executing scientifically useful virtual biomedical experiments. *Spring Simulation Multiconference*, Society for Computer Simulation International pp 697–706, San Diego, CA, USA.

Robert G Sargent (2007) Validation and verification of simulation models. IEEE *Winter Simulation Conference*, Simulation-A Bridge to the Future Vol. 1, pp. 39-48, Washington, DC, USA

Sheikh-Bahaei S, Maher JJ, and Anthony Hunt C (2010) Computational experiments reveal plausible mechanisms for changing patterns of hepatic zonation of xenobiotic clearance and hepatotoxicity. *J Theor Biol* 265:718–733.

Sheikh-Bahaei S, and Hunt CA (2011) Enabling clearance predictions to emerge from in silico actions of quasi-autonomous hepatocyte components. *Drug Metab Dispos* 39:1910–1920.

Smith AK, Petersen BK, Ropella GEP, Kennedy RC, Kaplowitz N, Ookhtens M, and Hunt CA (2016) Competing Mechanistic Hypotheses of Acetaminophen-Induced Hepatotoxicity Challenged by Virtual Experiments. *PLoS Comput Biol* 12:e1005253.

Smith AK, Xu Y, Ropella GEP, and Hunt CA (2018) A Model Mechanism-Based Explanation of an In

Vitro-In Vivo Disconnect for Improving Extrapolation and Translation. *J Pharmacol Exp Ther* 365:127–138.

Smith AK, Ropella GEP, McGill MR, Krishnan P, Dutta L, Kennedy RC, Jaeschke H, and Hunt CA (2020) Contrasting model mechanisms of alanine aminotransferase (ALT) release from damaged and necrotic hepatocytes as an example of general biomarker mechanisms. *PLoS Comput Biol* 16:e1007622.

Teutsch HF, Schuerfeld D, and Groezinger E (1999) Three-dimensional reconstruction of parenchymal units in the liver of the rat. *Hepatology* 29:494–505.

Teutsch HF (2005) The modular microarchitecture of human liver. *Hepatology* 42:317–325.

Wood FL, Houston JB, and Hallifax D (2017) Clearance Prediction Methodology Needs Fundamental Improvement: Trends Common to Rat and Human Hepatocytes/Microsomes and Implications for Experimental Methodology. *Drug Metab Dispos* 45:1178–1188.

Wood FL, Houston JB, and Hallifax D (2018) Importance of the Unstirred Water Layer and Hepatocyte Membrane Integrity In Vitro for Quantification of Intrinsic Metabolic Clearance. *Drug Metab Dispos* 46:268–278.

Yan L, Sheihk-Bahaei S, Park S, Ropella GEP, and Hunt CA (2008) Predictions of hepatic disposition properties using a mechanistically realistic, physiologically based model. *Drug Metab Dispos* 36:759–768.

## Footnotes

The research was funded by the UCSF BioSystems group.

Reprint Requests: C. Anthony Hunt

Address: Bioengineering and Therapeutic Sciences, 513 Parnassus Ave., HSE-1119, University of California, San Francisco, CA 94143-0912

email: a.hunt@ucsf.edu

## Figure Legends

**Figure. 1**. Virtual Rat components. (A) A vRat. (B) A portion of vLobule. Graph edges (red) designate flow connections within and between Layers. (C) A multi-layered, quasi-3D Sinusoidal Segment (SS) maps to a portion of lobular tissue. It comprises a Core surrounded concentrically by the five 2D grids described in the text. Mobile vCompound objects move within and between these grids. (D) Each Cell controls vCompound entry from and exit to an adjacent space.

**Figure. 2**. Relative PV-to-CV vHPC density within vLobules and vCulture configuration. (A) The height of each bar represents the mean number of vHPCs at the indicated vLobule location averaged over several Experiments. Moving left-to-right, the first 14 bars are located at increasing distances from PV (dPV) along the average PV-to-CV path. Moving right-to-left, the first 10 bars are located at increasing distances from CV (dCV) along the average CV-to-PV path. To characterize PV-to-CV differences in events, we average measures within the Periportal, Centrilobular, and Pericentral bands. (B) A vCulture comprises a Media Space plus a Layer (Layer 0) of reduced SS objects. The well-mixed Media Space functions the same as Rat Body. All vCulture SS are the same size.

**Figure. 3**. Measures of vC1 recorded during vCulture Experiments. A different *pEnter* value influences vCompound dynamics during each Experiment. Temporal values here, and in the following figures, are centered moving averages spanning 181 TS. (A) Percent Dose in Media space for each *pEnter*. (B) Mean Exposure rates per vHPC and (right) corresponding mean dynamic steady-state values for each *pEnter*. (C) Percent Dose in vHPCs and (right) corresponding mean dynamic steady-state values for each *pEnter*.

**Figure. 4**. Measures of vC1 recorded during vRat Experiments. (A) Percent Dose in Rat Body for each *pEnter*. (B) Mean Exposure rates per vHPC and (right) corresponding mean dynamic steady-state values for each *pEnter*. (C) Percent Dose in vHPCs and (right) corresponding mean dynamic steady-state values for each *pEnter*. (D) Mean dynamic steady-state values for vHPC Exposure rates within the Periportal (PP), Centrilobular (CL), and Pericentral (PC) bands (Fig. 2A) for each *pEnter*. (E) Amounts within the three bands for each *pEnter*. (F) Mean dynamic steady-state amounts per vHPCs within the three bands for each *pEnter*.

**Figure. 5**. Measures of vC2 recorded during six vCulture Experiments. (A) Percent Dose in Media space for each *pEnter*. (B) Mean Removal rates per vHPC and (right) corresponding mean (spanning 3,000 TS) peak Removal rates for each *pEnter*. (C) Extraction ratio and (right) corresponding mean dynamic steady-state values for each *pEnter*. Measures for *pEnter* = 1.0 and 0.8 terminate because (essentially) all vC2 has been removed. (D) Percent Dose in vHPCs for each *pEnter*. Insert: mean values at $t$ = 3,000 TS for each *pEnter*.

**Figure. 6**. Measures of vC2 recorded during six vRat Experiments. (A) Percent Dose in Rat Body for each *pEnter*. (B) Mean Removal rates per vHPC and (right) corresponding mean peak (spanning 3,000 TS) Removal rates for each *pEnter*. To facilitate comparisons between vCulture and vRat results, the blue curve traces the corresponding mean peak Removal rates from Fig. 5B. (C) Extraction ratio following execution and (right) corresponding mean dynamic steady-state values for each *pEnter*. Measures for *pEnter* = 0.2-1.0 terminate because (essentially) all vC2 has been removed. (D) Percent Dose in vLiver for each *pEnter*. (E) Mean peak vHPC Removal rates (calculated as in B) within the PP, CL, and PC bands (Fig. 2A). (F) Percent Dose within PP, CL, and PC bands at $t$ = 7,500 TS. (G) Percent Dose per vHPC within PP, CL, and PC bands at $t$ = 7,500 TS.

**Figure. 7**. The four-stage working thesis. (A) An IVIVE method underpredicts a drug's hepatic clearance. Why? (B) Establish quantitative mappings between measures of a vCompound during vCulture Experiments and the target drug's in vitro clearance. (C) Establish quantitative mappings between measures of that same vCompound during vRat Experiments and hepatic clearance. (D) Compare and contrast details of vCompound's removal during vRat and vCulture Experiments. Posit a concrete explanation for the underprediction.

## Figures

Figure 1

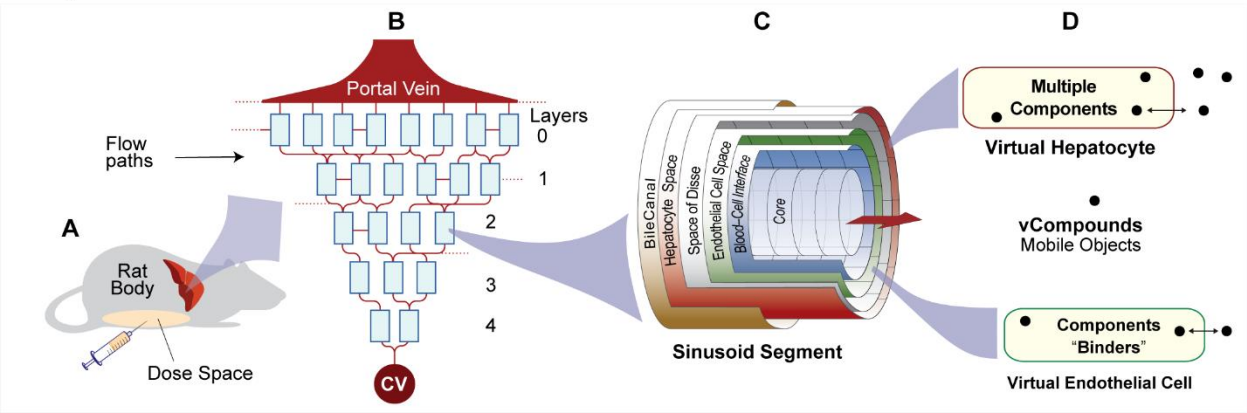

Figure 2

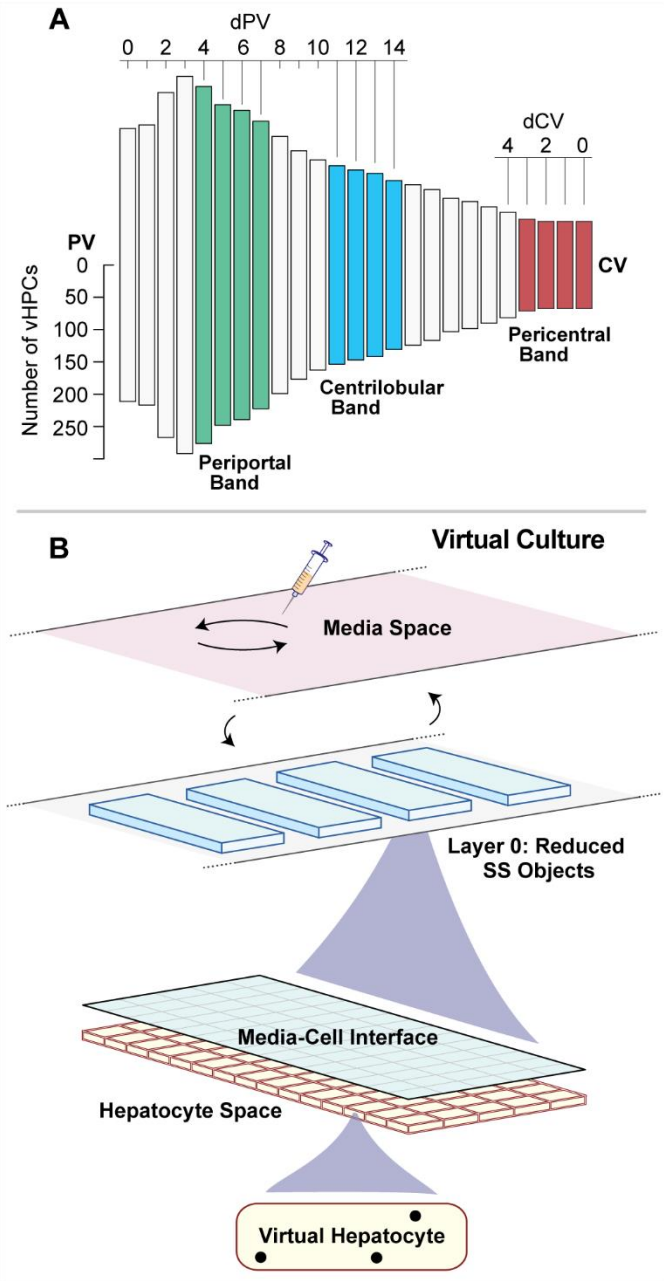
A
dPV
0 2 4 6 8 10 12 14
dCV
4 2 0
PV
0
50
100
150
200
250
Number of vHPCs
CV
Pericentral Band
Centrilobular Band
Periportal Band
B
Virtual Culture
Media Space
Layer 0: Reduced SS Objects
Media-Cell Interface
Hepatocyte Space
Virtual Hepatocyte

**Figure 3**

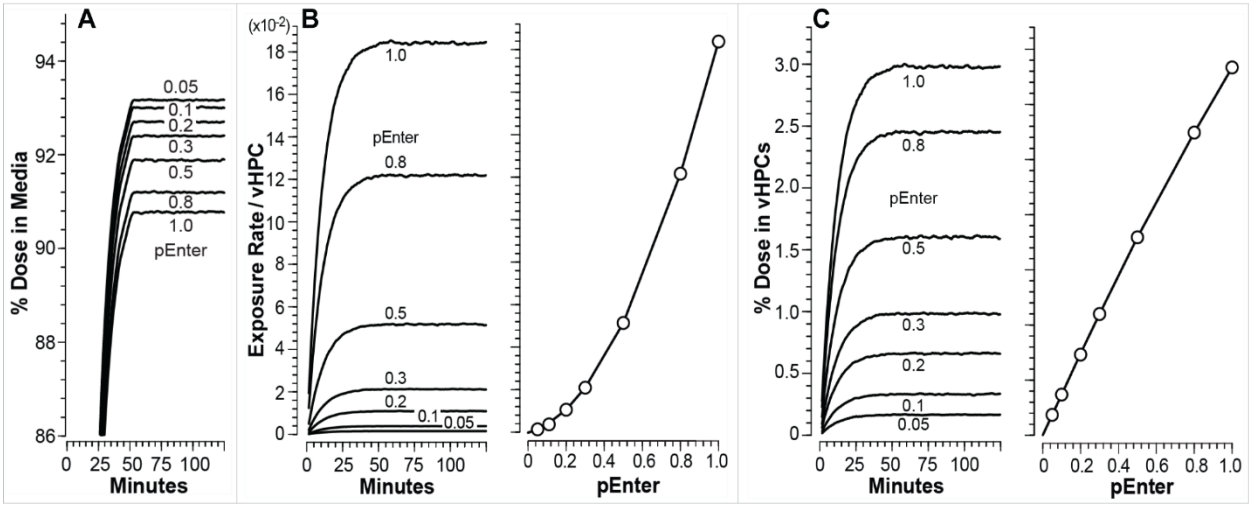
A
% Dose in Media
94
92
90
88
86
0.05
0.1
0.2
0.3
0.5
0.8
1.0
pEnter
0 25 50 75 100
Minutes
B
(x10-2)
Exposure Rate / vHPC
18
16
14
12
10
8
6
4
2
0
1.0
pEnter
0.8
0.5
0.3
0.2
0.1
0.05
0 25 50 75 100
Minutes
0 0.2 0.4 0.6 0.8 1.0
pEnter
C
% Dose in vHPCs
3.0
2.5
2.0
1.5
1.0
0.5
0
1.0
0.8
pEnter
0.5
0.3
0.2
0.1
0.05
0 25 50 75 100
Minutes
0 0.2 0.4 0.6 0.8 1.0
pEnter

**Figure 4**

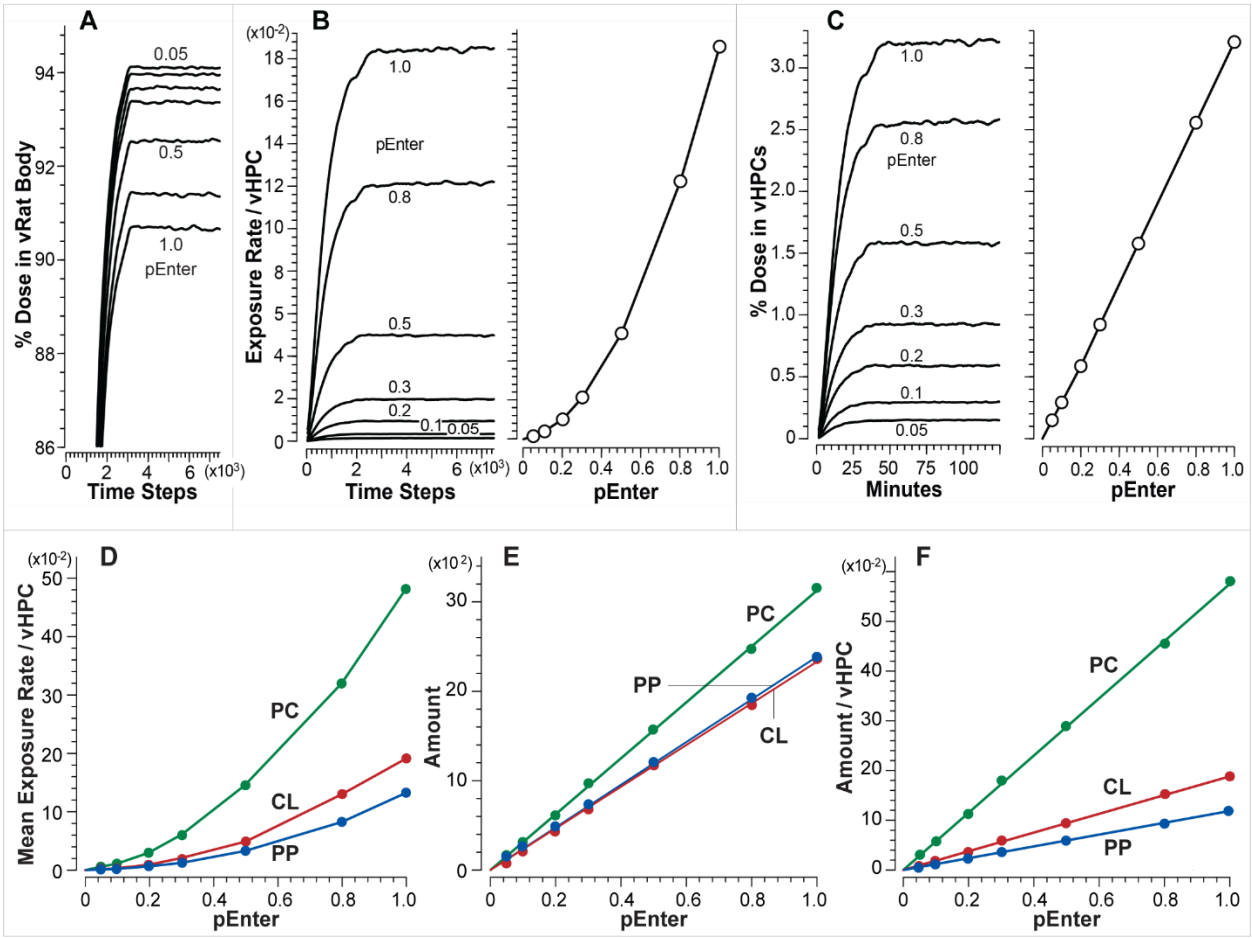
A
% Dose in vRat Body
Time Steps
0.05
0.5
1.0
pEnter
B
Exposure Rate / vHPC
Time Steps
pEnter
1.0
0.8
0.5
0.3
0.2
0.1
0.05
C
% Dose in vHPCs
Minutes
pEnter
1.0
0.8
0.5
0.3
0.2
0.1
0.05
D
Mean Exposure Rate / vHPC
pEnter
PC
CL
PP
E
Amount
pEnter
PC
PP
CL
F
Amount / vHPC
pEnter
PC
CL
PP

**Figure 5**

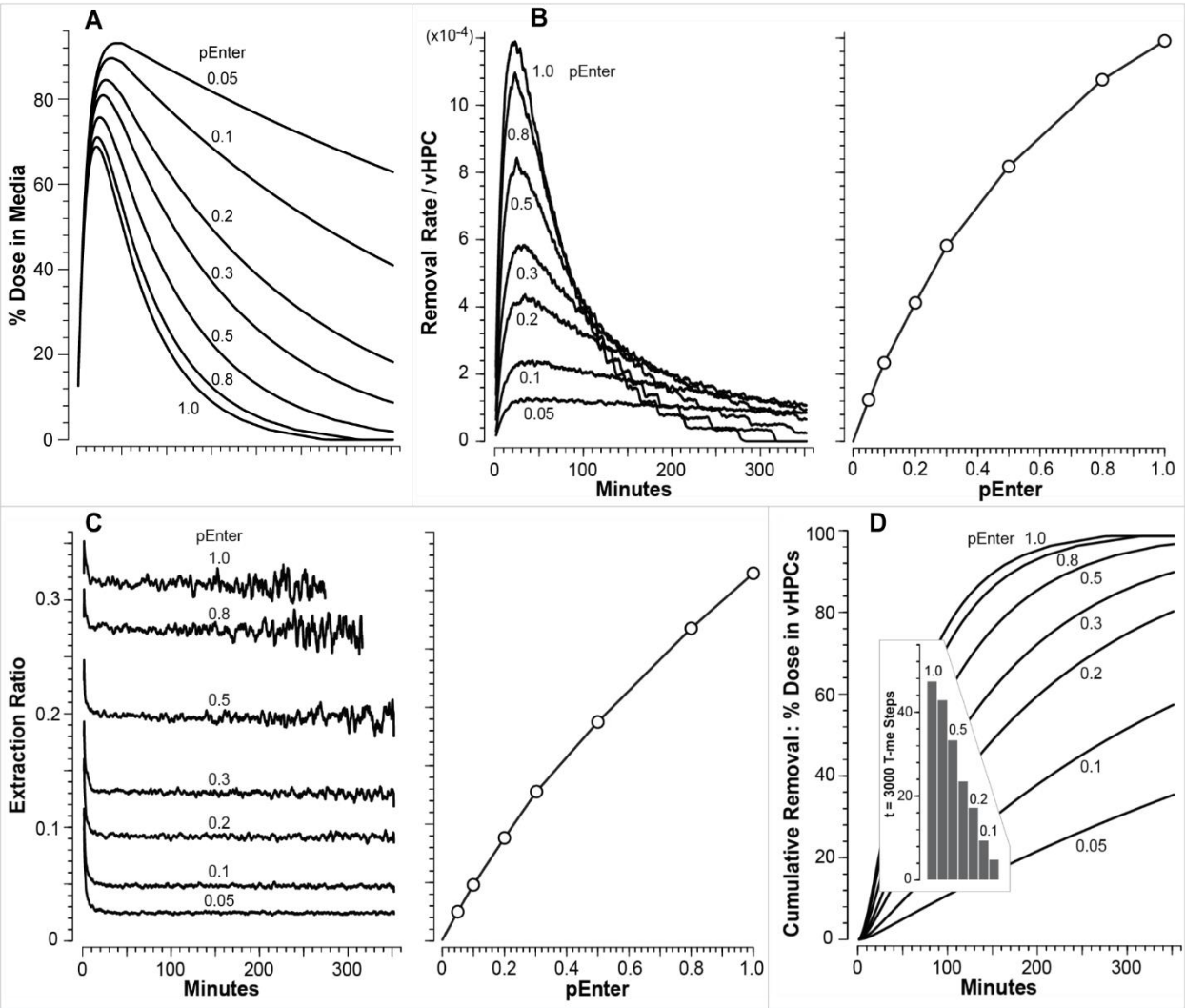
A
pEnter
0.05
0.1
0.2
0.3
0.5
0.8
1.0
% Dose in Media
B
(x10-4)
1.0 pEnter
0.8
0.5
0.3
0.2
0.1
0.05
Removal Rate / vHPC
Minutes
pEnter
C
pEnter
1.0
0.8
0.5
0.3
0.2
0.1
0.05
Extraction Ratio
Minutes
pEnter
D
pEnter 1.0
0.8
0.5
0.3
0.2
0.1
0.05
t = 3000 T-me Steps
Cumulative Removal : % Dose in vHPCs
Minutes

Figure 6

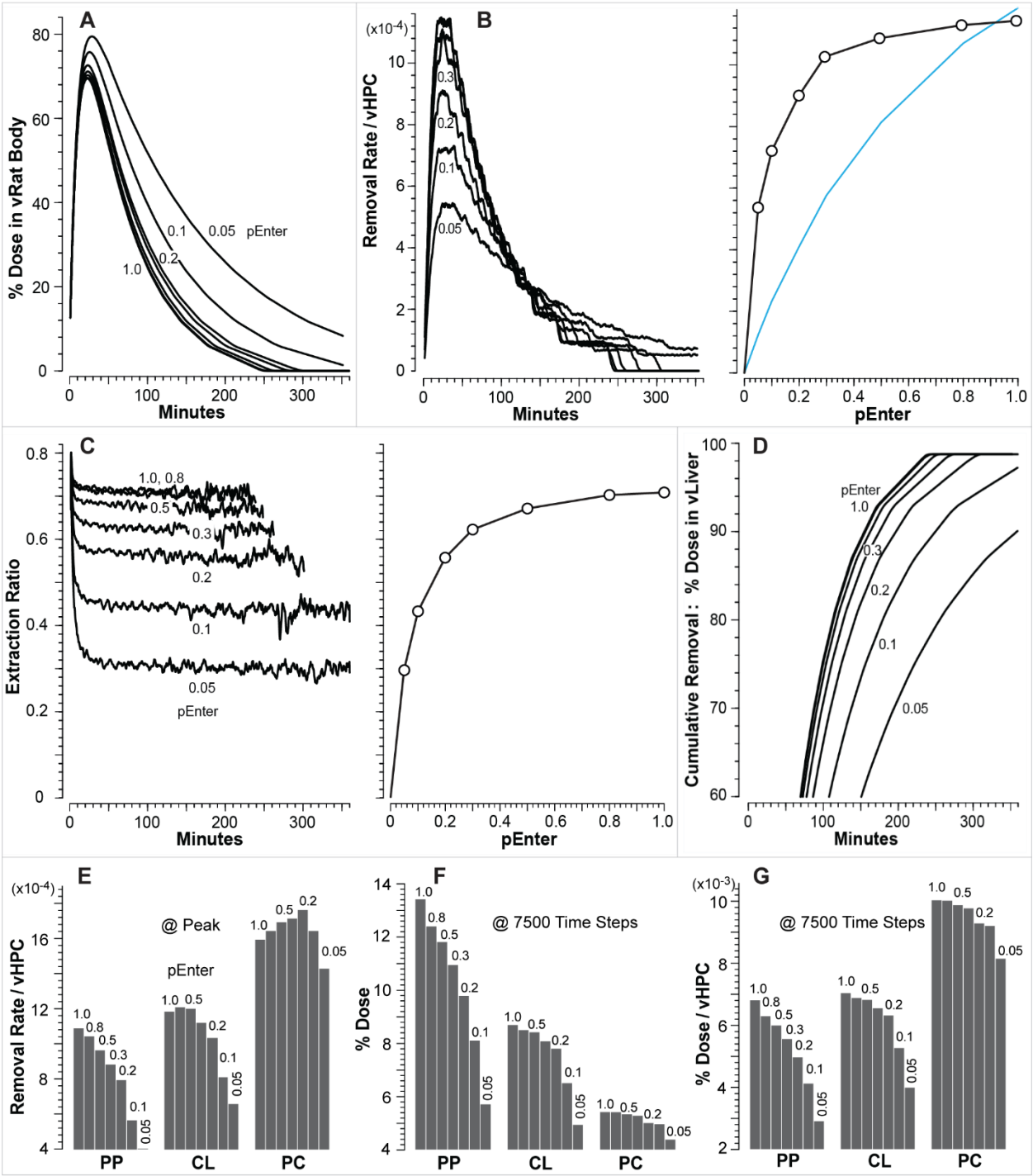
A
% Dose in vRat Body
Minutes
1.0
0.2
0.1
0.05
pEnter
B
(x10-4)
Removal Rate / vHPC
Minutes
0.3
0.2
0.1
0.05
pEnter
C
Extraction Ratio
Minutes
1.0, 0.8
0.5
0.3
0.2
0.1
0.05
pEnter
D
Cumulative Removal : % Dose in vLiver
Minutes
pEnter
1.0
0.3
0.2
0.1
0.05
E
(x10-4)
Removal Rate / vHPC
@ Peak
pEnter
PP
CL
PC
F
% Dose
@ 7500 Time Steps
PP
CL
PC
G
(x10-3)
% Dose / vHPC
@ 7500 Time Steps
PP
CL
PC
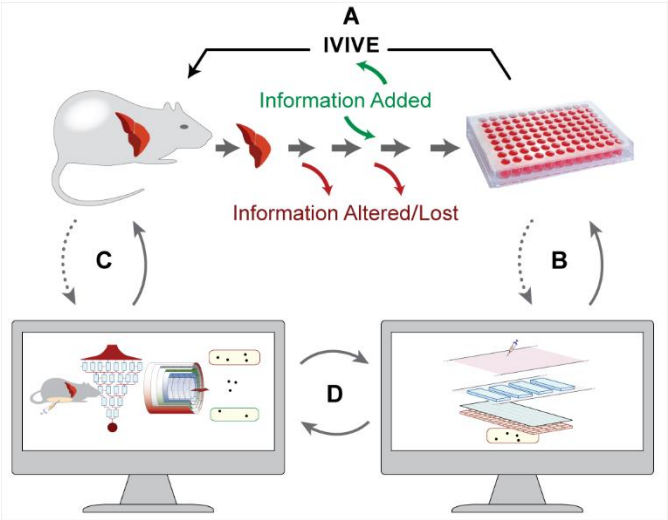
**Figure 7**